

1 **Supporting Information**

2 *for*

3 **Measurement report: Aerosol and cloud nuclei properties along the Central and**  
4 **Northern Great Barrier Reef: Impact of anthropogenic emissions**

5 E. Johanna Horchler<sup>1,\*</sup>, Joel Alroe<sup>1</sup>, Luke Harrison<sup>2</sup>, Luke Cravigan<sup>1</sup>, Daniel P. Harrison<sup>2,3</sup>,  
6 Zoran D. Ristovski<sup>1</sup>

7  
8 <sup>1</sup>International Laboratory for Air Health and Quality, Queensland University of Technology, Brisbane, 4001,  
9 Australia

10 <sup>2</sup>National Marine Science Centre, Southern Cross University, Coffs Harbour, 2450, Australia

11 <sup>3</sup>School of Geosciences, University of Sydney, Sydney 2006, Australia

12 \*Now at: Department of Chemistry, Faculty of Natural Science, Aarhus University, Aarhus C, 8000, Denmark

13 *Correspondence to:* Eva Johanna Horchler (eva.horchler@qut.edu.au)

14  
15 **S1. Details on the instrumental set-up and data analysis**

16 Particle number concentration ( $> 7$  nm) and size distribution were obtained using a Mixing  
17 Condensation Particle Counter (mCPC 1720, Brechtel Manufacturing Inc.), a Scanning  
18 Electrical Mobility Spectrometer (SEMS 2100, Brechtel Manufacturing Inc.) combined with a  
19 mCPC 1720, and an Aerodynamic Particle Sizer (APS 3321, TSI Inc.). The SEMS was  
20 operated at a sheath flow rate of  $5 \text{ L min}^{-1}$  and set to scan 150 aerosol diameter bins from 5 to  
21 1081 nm, in both up and down scanning modes, with a 5-minute scan time. The APS captured  
22 size distributions from 0.5 to  $5 \mu\text{m}$ , with a time resolution of 2 minutes. The APS data was  
23 exported with Stokes correction turned on and an assumed density of  $1.3 \text{ g cm}^{-3}$ . The density  
24 was chosen under the assumption that the particles are composed of sea salt and an inlet relative

25 humidity of approximately 50 %. APS measurements for particle diameters less than 700 nm  
26 were removed due to known measurement biases at these diameters (Beddows et al., 2010).  
27 APS aerodynamic diameters were converted to the volume equivalent diameter (DeCarlo et al.,  
28 2004). The particle density required for the conversion was modelled as a function of relative  
29 humidity using E-AIM (Wexler and Clegg, 2002) and an assumed particle composition of NaCl  
30 with  $1.3 \text{ g cm}^{-3}$  at 50 % RH. The APS and SEMS diameters were further corrected for the  
31 relative humidity dependent growth factor (GF), which is computed taking the measured RH  
32 by the SEMS, and assuming a composition of ammonium sulfate for the SEMS and sea salt for  
33 the APS based on the size-dependent chemical composition typically observed in marine sea  
34 spray aerosols (Heintzenberg et al., 2000). In the absence of RH data, an RH of 48 % was  
35 estimated as the average value across the entire period. The APS and SEMS data were corrected  
36 for size-dependent inlet losses (Fig. S1), combined into a single size distribution ranging from  
37 5 nm to 5000 nm and re-binned onto a 32-channel per decade set of particle diameters.  
38 Overlapping bins were averaged. Due to instrument artifacts, concentrations for particles  
39 smaller than 10 nm were not reliable and thus were not considered.

40

41 The CCN-100 measured the total CCN number concentration at a range of supersaturations  
42 (0.1 %, 0.2 %, 0.3 %, 0.5 %, 0.7 % for 10 minutes each). The data are processed to remove the  
43 first 150 seconds of data at supersaturations 0.2 to 0.7 % and 300 seconds at 0.1 %

44 supersaturation to ensure that the supersaturation has stabilised in the instrument. The  $\kappa$ -Köhler  
45 model was used to determine the hygroscopicity parameter for the background aerosol (Petters  
46 and Kreidenweis, 2007). Therefore, the critical diameter for cloud droplet activation was  
47 determined by integrating the size distribution, from the largest diameter to the diameter at  
48 which the integration is equal to the measured CCN number concentration at the measured  
49 supersaturation. The measured CCN was taken as the average of the CCN measured during the  
50 averaging period for the size distribution. The measurement uncertainty in the computed  
51 critical diameter was computed as a sum of the standard deviation in the mean of the CCN  
52 number concentrations and the relative uncertainty in the size distribution. The size distribution  
53 uncertainty was assumed to be equal to the standard deviation in the mean of the CPC  
54 concentrations over the averaging period, which assumes that the uncertainty in the distribution  
55 is not dependent on particle diameter. The hygroscopicity parameter was then computed for  
56 the above calculated critical diameter (Petters and Kreidenweis, 2007). The Hoppel Minimum,  
57 which is formed due to the in-cloud growth of aerosol, was calculated as the global minimum  
58 between 30 nm and 150 nm if present. The corresponding effective maximum in-cloud  
59 supersaturation at the Hoppel minimum can be approximated via  $\kappa$ -Köhler theory using the  
60 hygroscopicity parameter  $\kappa$  (Gong et al., 2023).

61

62 The time zone was set to UTC time for all measurements. The times were adjusted for time  
63 delays between the individual instruments. For comparison reasons, all instruments, except the  
64 SEMS were averaged onto the same timescale of one hour unless stated otherwise.

65

66 NOAA's Hybrid-Single-Particle Lagrangian Integrated Trajectory (HYSPLIT) dispersion  
67 model (Stein et al., 2015) was used to calculate back trajectories, representing the path taken  
68 by each air mass during the three days prior to reaching the ship. Because air masses that passed  
69 over land within three days before reaching the ship showed a clear land signature, but  
70 associated HYSPLIT back-trajectory errors are proportional to 15 to 30 % of the trajectory  
71 travel distance (Draxler and Rolph, 2007), the back-trajectory duration was thus limited to three  
72 days. The dispersion model was underpinned by meteorological data obtained from the Global  
73 Data Assimilation System (GDAS) dataset at 1° spatial resolution. To ensure that the trajectory  
74 starting height is representative of the airmass pathways, starting heights of 0.5 of the planetary  
75 boundary layer (PBL) height, and 10 m above mean sea level, which corresponds to the  
76 sampling inlet height, were evaluated. Because both approaches yield similar trajectories, a  
77 starting height of 10 m above sea level was chosen to account for the actual sampling height  
78 and allow for greater variations in the vertical dimension within the PBL. This is required for  
79 the calculation of HYSPLIT ensemble trajectories, which apply small spatial perturbations  
80 based on user-defined grid offsets to the end point prior to estimating the trajectories. In this

81 study for each hour of sampling, an ensemble of 27 trajectories was generated. Each ensemble  
82 was then averaged to give a trajectory that best represented the path taken by the air mass. To  
83 identify periods that may have been influenced by continental emissions, continental  
84 boundaries were sourced from the ArcGIS Hub (Esri, 2021). Any air masses that passed over  
85 land within three days of reaching the ship were classified as “continental”.

86

87

88

89

90

91

92

93

94

95

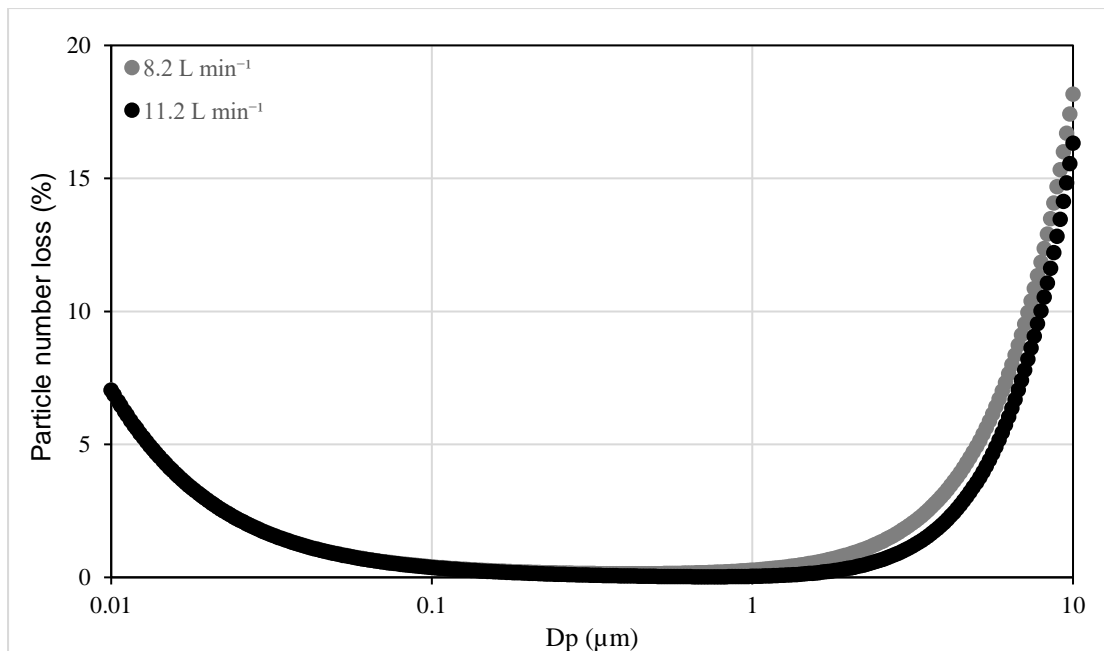
96



104

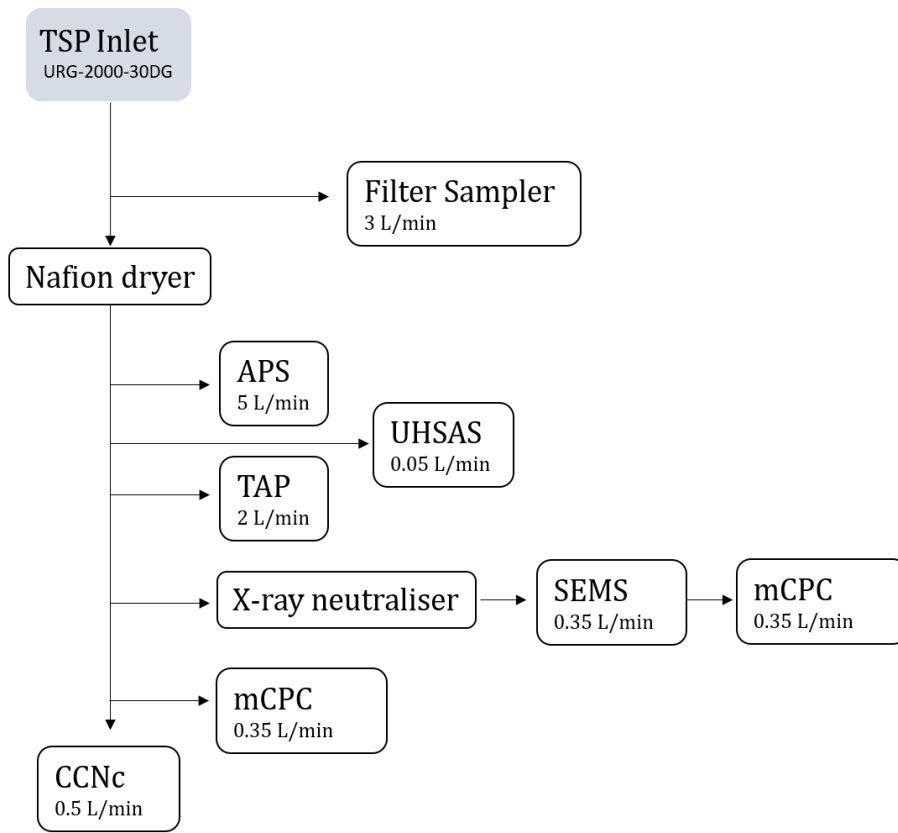
105 **Figure S1.** (a) Exterior of the Cloud-Cube (b) data logging, inlet control systems, UHSAS,

106 filter sampler, airconditioner (c) APS, SEMS, TAP, CPC's and CCNc.



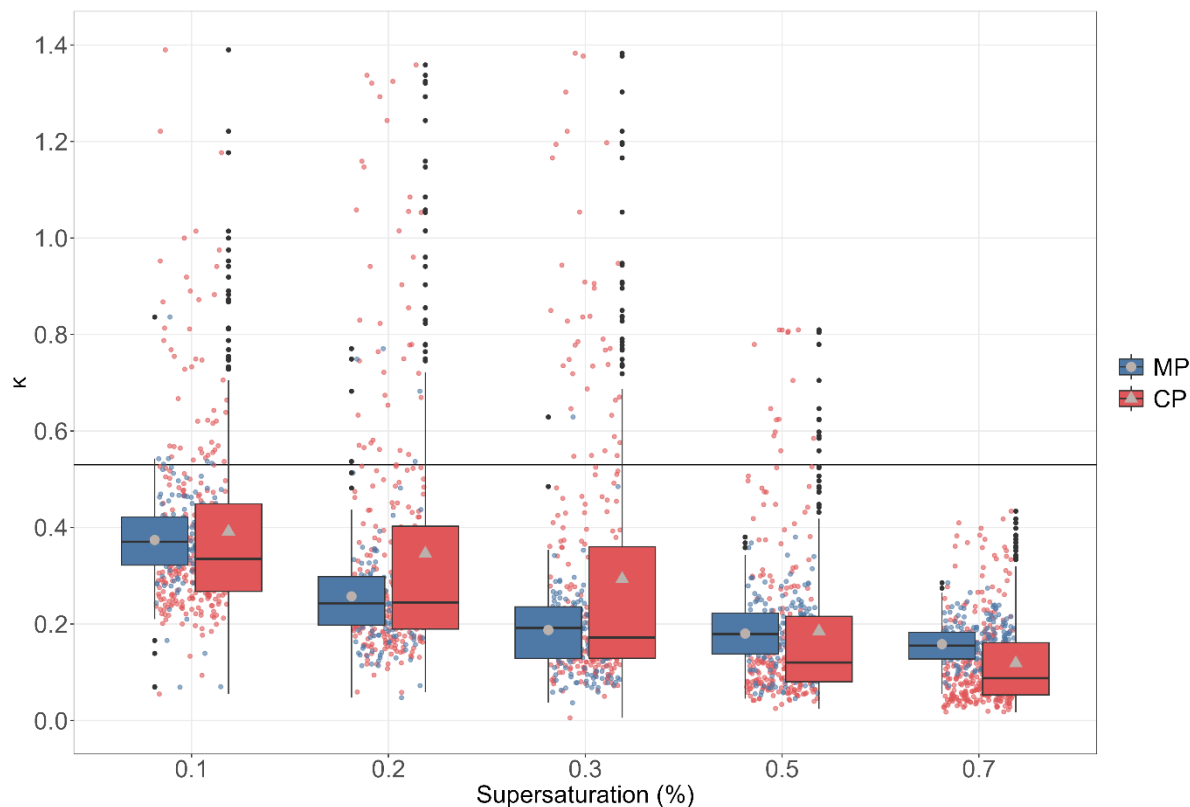
107

108 **Figure S2.** Particle number loss as a function of diameter for the aerosol sampling equipment  
 109 during the Atmospheric Survey in February and March 2022 as modelled using the Particle  
 110 Loss Calculator. All instruments running together made up a total flow rate of 11.2 L min<sup>-1</sup>. In  
 111 the case where the filter sampler was not running, the total flow rate was 8.2 L min<sup>-1</sup>. The  
 112 corresponding particle loss correction was applied for each flow rate, even though differences  
 113 in the particle losses are only significant for supermicron particles.



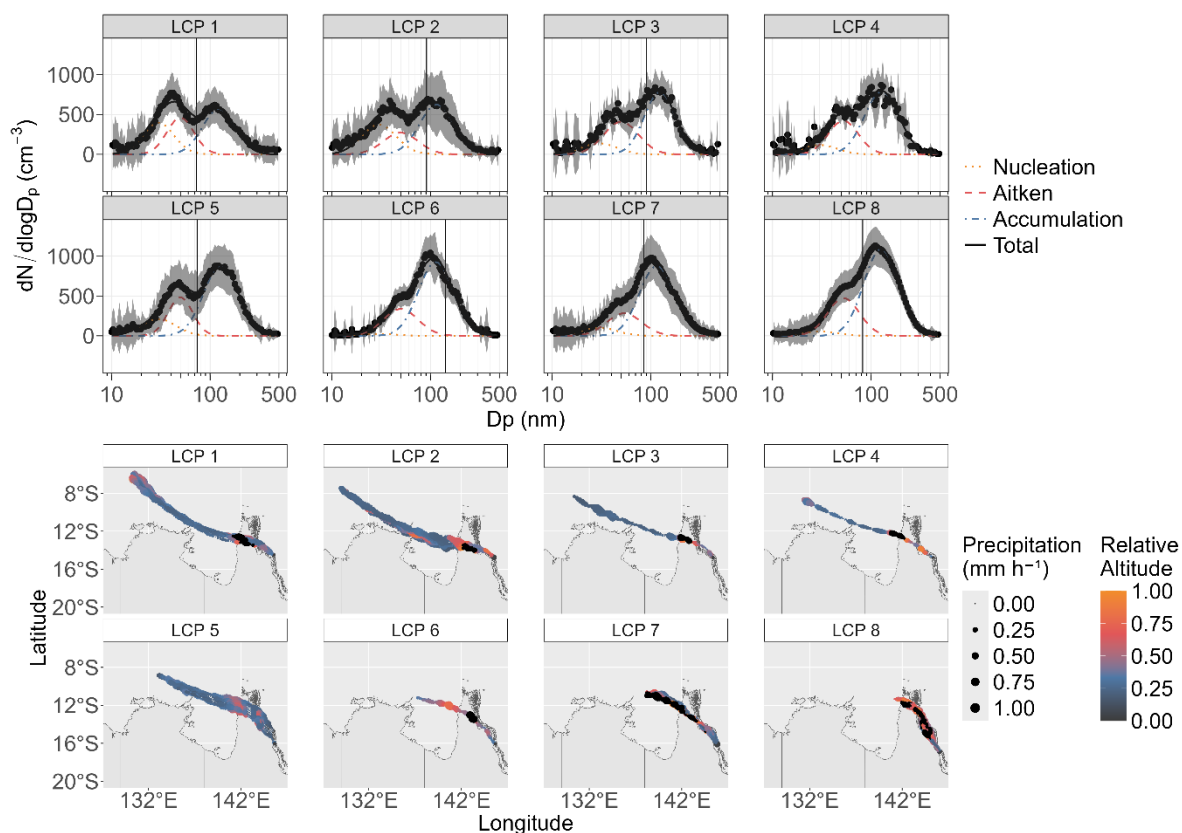
114

115 **Figure S3.** Schematic of the set-up. Arrows indicate the flow directions.



116

117 **Figure S4.** Aerosol hygroscopicity parameters  $\kappa$  for the MP (blue) and CP (red) averaged on a  
 118 minute timeframe at different supersaturations. The black horizontal line at 0.53 indicates the  
 119 hygroscopicity parameter  $\kappa$  for pure ammonium sulfate (Petters and Kreidenweis, 2007). The  
 120 black horizontal line in a box displays the median of the individual data. The lower and upper  
 121 hinges represent the 25<sup>th</sup> and 75<sup>th</sup> percentiles. The upper and lower whiskers extend from the  
 122 hinge to the largest or smallest measured values, respectively, but not more than 1.5 times the  
 123 difference between the 25<sup>th</sup> and 75<sup>th</sup> percentiles. The mean is shown as grey points for the MP  
 124 and grey triangles for the CP. Outliers are individual data points that fall outside of this range  
 125 and are color-coded black.



126

127 **Figure S5.** Average aerosol number size distributions (top) and the three-day back-trajectories  
 128 (bottom) for the eight continental low CN number concentration periods (LCP1-8). The lines  
 129 in the size distribution plots represent lognormal fits for the nucleation mode (dotted orange),  
 130 Aitken mode (dashed red), accumulation mode (dot-dashed blue), and total (solid black). The  
 131 black vertical line indicates the critical diameter ( $D_{\text{crit}}$ ). No CCN data for 0.3% SS were  
 132 available during LCP4. Back-trajectories are coloured by their altitude in respect to the  
 133 planetary boundary layer height. Black data points represent air masses travelling through the  
 134 free troposphere. The precipitation amount determines the size of the trajectory points. The  
 135 ship location marks the start point of each trajectory. The GBR was provided in the gisaimsr  
 136 package by the Geoscience Australia (GA) and the Great Barrier Reef Marine Park Authority

137 (GBRMPA). The continental boundaries were obtained from the ozmaps package  
138 (doi:10.32614/CRAN.package.ozmaps).

139

140

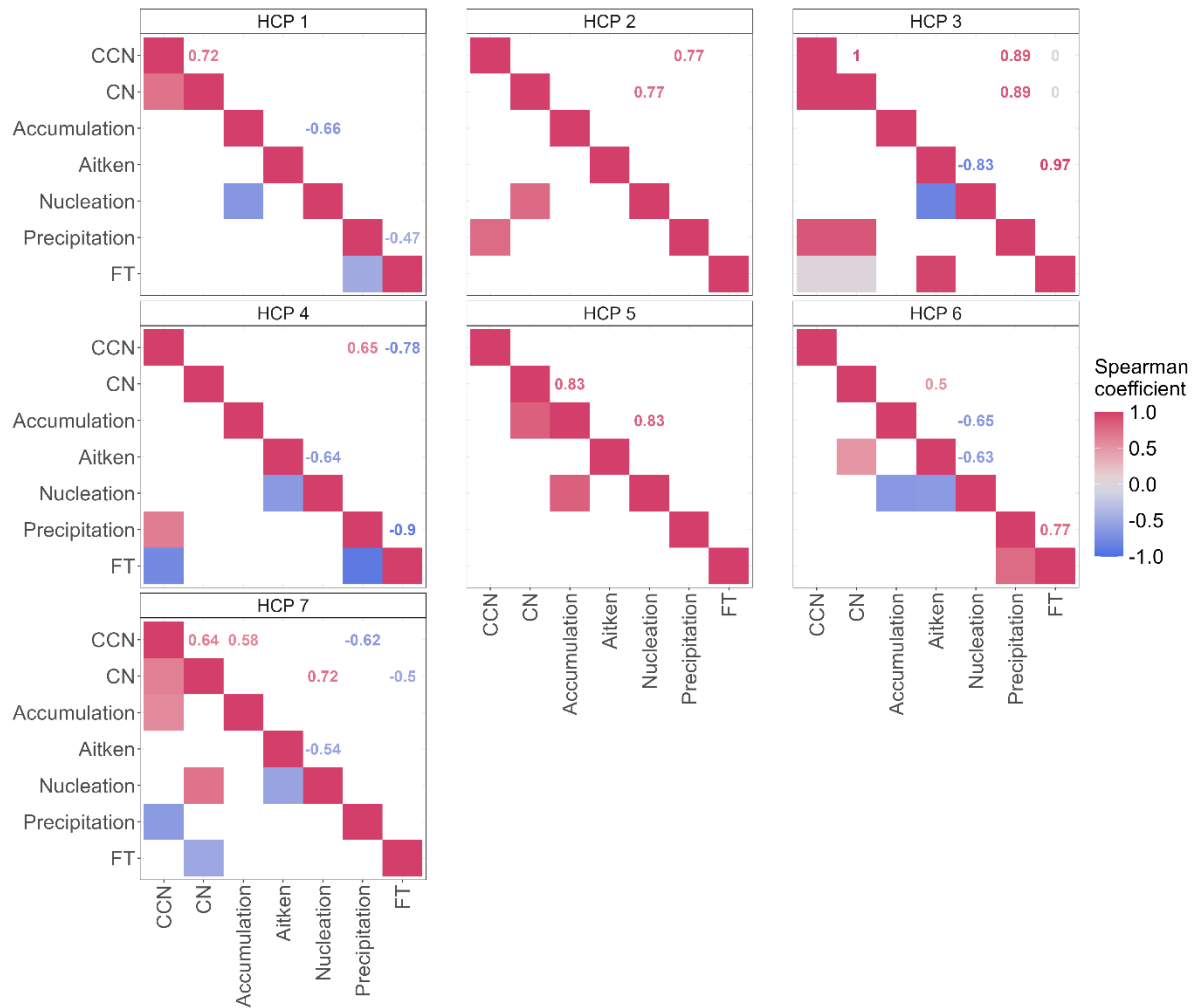
141

142

143

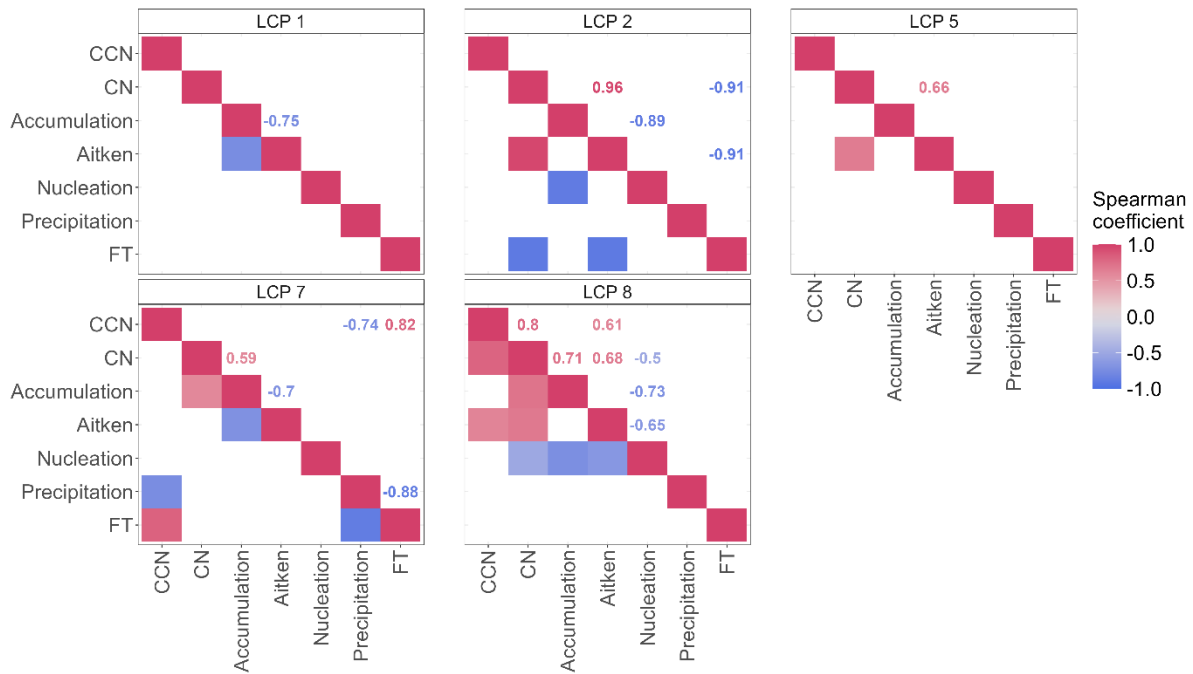
144

145



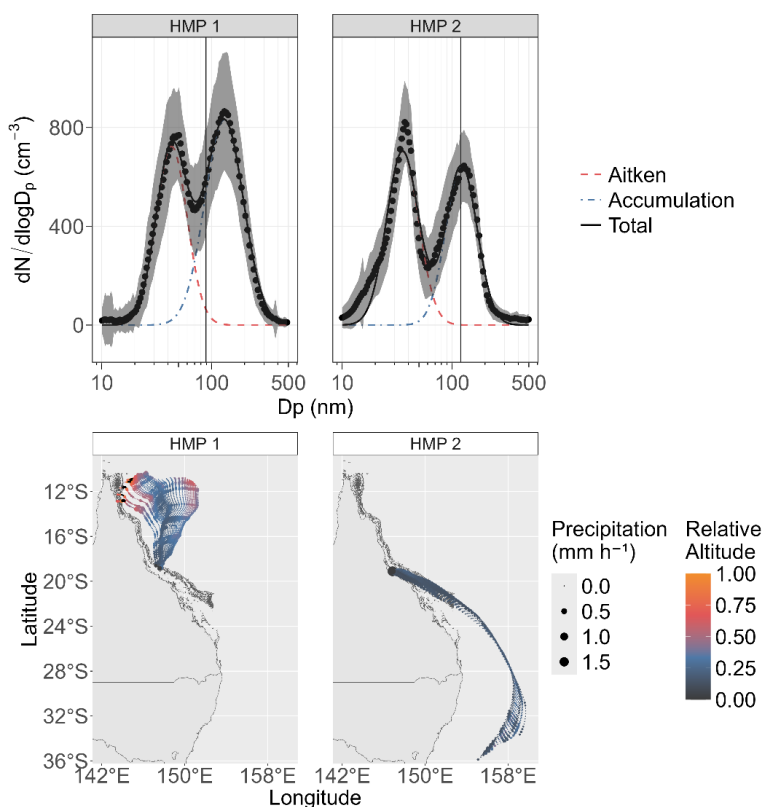
146

147 **Figure S6:** Spearman correlation coefficient ( $p < 0.05$ ) between CCN number concentration,  
 148 CN number concentration inferred from the total fit, number concentration in the accumulation  
 149 mode, number concentration in the Aitken mode, number concentration in the nucleation mode,  
 150 averaged precipitation along one trajectory, and the percentage of time the trajectory spent in  
 151 the FT for the seven continental high CN number concentration periods (HCP1-7).



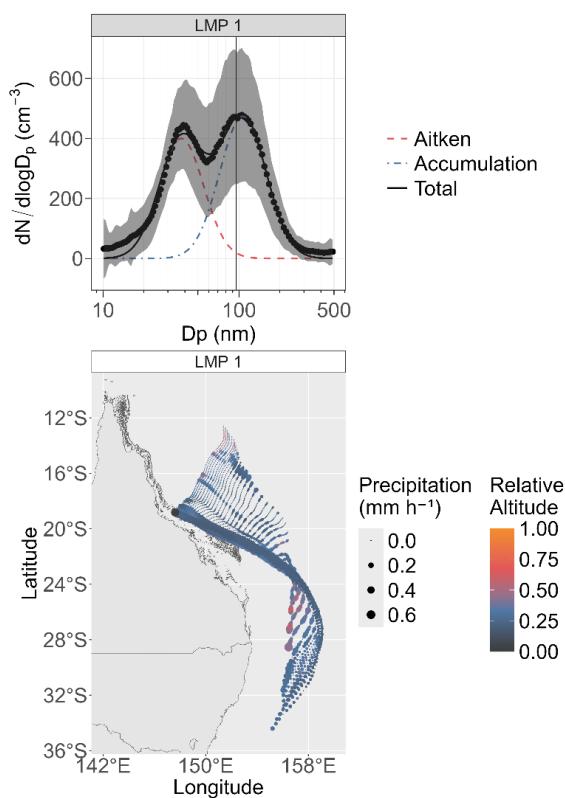
152

153 **Figure S7:** Spearman correlation coefficient ( $p < 0.05$ ) between CCN number concentration,  
 154 CN number concentration inferred from the total fit, number concentration in the accumulation  
 155 mode, number concentration in the Aitken mode, number concentration in the nucleation mode,  
 156 averaged precipitation along one trajectory, and the percentage of time the trajectory spent in  
 157 the FT for five continental low CN number concentration periods (LCP1-2, LCP5, LCP7-8).  
 158 LCP3-4, and LCP6 do not include enough data points to perform a correlation analysis.



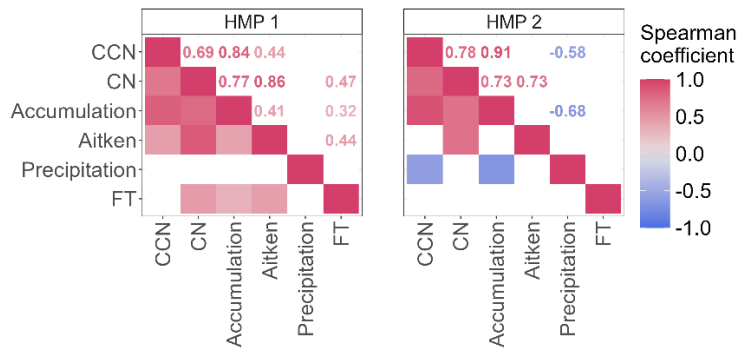
159

160 **Figure S8.** Average aerosol number size distributions (top) and the three-day back-trajectories  
 161 (bottom) for the two marine high CN number concentration periods (HMP1-2). The lines in  
 162 the size distribution plots represent lognormal fits for the nucleation mode (dotted orange),  
 163 Aitken mode (dashed red), accumulation mode (dot-dashed blue), and total (solid black). The  
 164 black vertical line indicates the critical diameter ( $D_{\text{crit}}$ ). Back-trajectories are coloured by their  
 165 altitude in respect to the planetary boundary layer height. Black data points represent air masses  
 166 travelling through the free troposphere. The precipitation amount determines the size of the  
 167 trajectory points. The ship location marks the start point of each trajectory. The GBR was  
 168 provided in the gisaimsr package by the Geoscience Australia (GA) and the Great Barrier Reef  
 169 Marine Park Authority (GBRMPA). The continental boundaries were obtained from the  
 170 ozmaps package (doi:10.32614/CRAN.package.ozmaps).



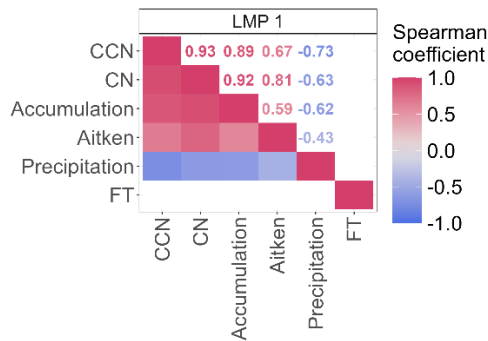
171

172 **Figure S9.** Average aerosol number size distributions (top) and the three-day back-trajectories  
 173 (bottom) for the marine low CN number concentration periods (LMP1). The lines in the size  
 174 distribution plots represent lognormal fits for the nucleation mode (dotted orange), Aitken  
 175 mode (dashed red), accumulation mode (dot-dashed blue), and total (solid black). The black  
 176 vertical line indicates the critical diameter ( $D_{\text{crit}}$ ). Back-trajectories are coloured by their  
 177 altitude in respect to the planetary boundary layer height. Black data points represent air masses  
 178 travelling through the free troposphere. The precipitation amount determines the size of the  
 179 trajectory points. The ship location marks the start point of each trajectory. The GBR was  
 180 provided in the gisaimsr package by the Geoscience Australia (GA) and the Great Barrier Reef  
 181 Marine Park Authority (GBRMPA). The continental boundaries were obtained from the  
 182 ozmaps package (doi:10.32614/CRAN.package.ozmaps).



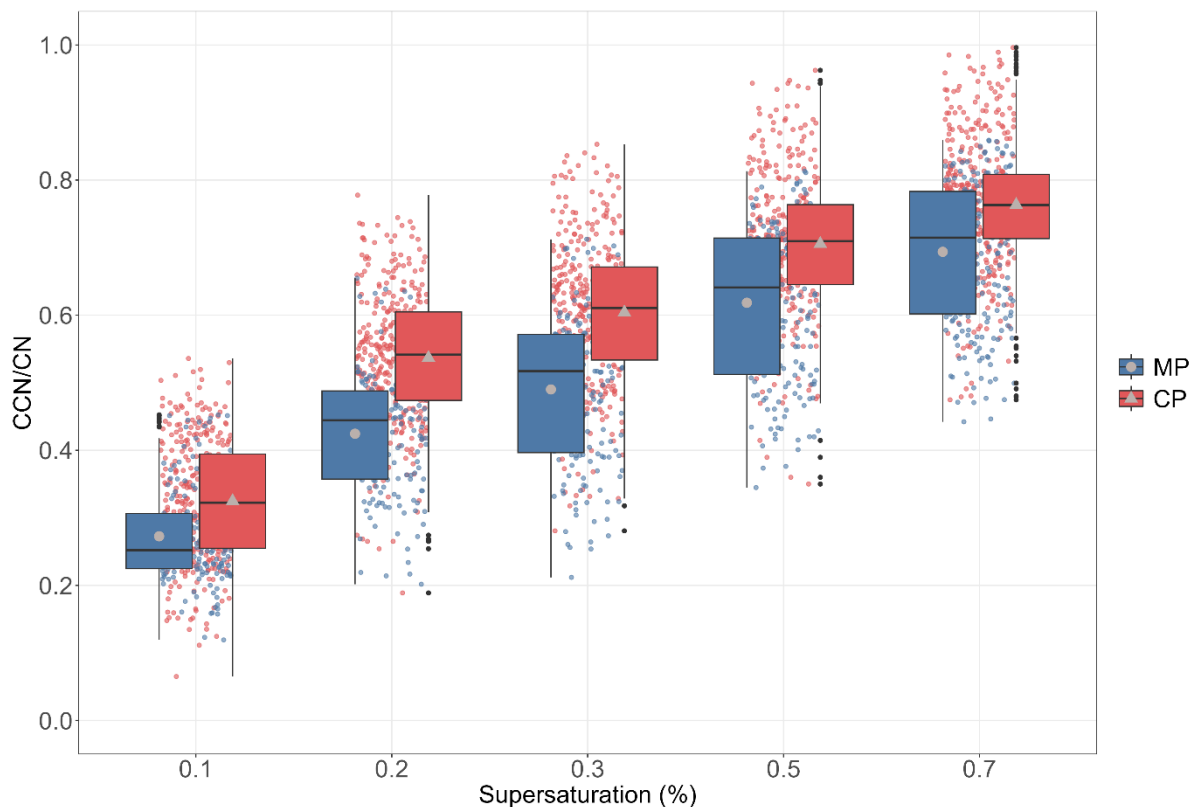
183

184 **Figure S10:** Spearman correlation coefficient ( $p < 0.05$ ) between CCN number concentration,  
 185 CN number concentration inferred from the total fit, number concentration in the accumulation  
 186 mode, number concentration in the Aitken mode, number concentration in the nucleation mode,  
 187 averaged precipitation along one trajectory, and the percentage of time the trajectory spent in  
 188 the FT for the two marine high CN number concentration periods (HMP1-2).



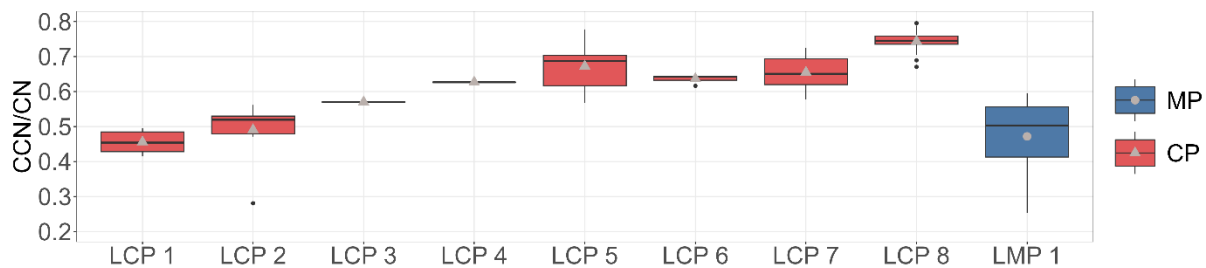
189

190 **Figure S11:** Spearman correlation coefficient ( $p < 0.05$ ) between CCN number concentration,  
 191 CN number concentration inferred from the total fit, number concentration in the accumulation  
 192 mode, number concentration in the Aitken mode, number concentration in the nucleation mode,  
 193 averaged precipitation along one trajectory, and the percentage of time the trajectory spent in  
 194 the FT for the marine low CN number concentration periods (LMP1).



195

196 **Figure S12.** CCN activation ratios  $CCN/CN$  for the MP (blue) and CP (red) averaged on a  
 197 minute timeframe at different supersaturations. The black horizontal line in a box displays the  
 198 median of the individual data. The lower and upper hinges represent the 25<sup>th</sup> and 75<sup>th</sup>  
 199 percentiles. The upper and lower whiskers extend from the hinge to the largest or smallest  
 200 measured values, respectively, but not more than 1.5 times the difference between the 25<sup>th</sup> and  
 201 75<sup>th</sup> percentiles. The mean is shown as grey points for the MP and grey triangles for the CP.  
 202 Outliers are individual data points that fall outside of this range and are color-coded black.



203

204 **Figure S13:** CCN activation ratios (CCN/CN) at 0.3 % SS for the MP (blue) and the CP (red)  
 205 for the low CN number concentration periods (LCP1-8 and LMP1). The black horizontal line  
 206 in a box displays the median of the individual data. The lower and upper hinges represent the  
 207 25<sup>th</sup> and 75<sup>th</sup> percentiles. The upper and lower whiskers extend from the hinge to the largest or  
 208 smallest measured values, respectively, but not more than 1.5 times the difference between the  
 209 25<sup>th</sup> and 75<sup>th</sup> percentiles. The mean is shown as grey points for the MP and grey triangles for  
 210 the CP. Outliers are individual data points that fall outside of this range and are color-coded  
 211 black.

212

213

214

215

216

217

218

219

220

221 **References**

- 222 1 Beddows, D. C. S., Dall'Osto, M., and Harrison, R. M.: An Enhanced Procedure for the  
223 Merging of Atmospheric Particle Size Distribution Data Measured Using Electrical  
224 Mobility and Time-of-Flight Analysers, *Aerosol Sci. Technol.*, 44:11, 930-938,  
225 doi:10.1080/02786826.2010.502159, 2010.
- 226 2 Conrad, B. M. and Johnson, M. R.: Mass absorption cross-section of flare-generated black  
227 carbon: Variability, predictive model, and implications. *Carbon*, 149, 760-771,  
228 doi:10.1016/j.carbon.2019.04.086, 2019.
- 229 3 DeCarlo, P. F., Slowik, J. G., Worsnop, D. R., Davidovits, P., and Jimenez, J. L.: Particle  
230 Morphology and Density Characterization by Combined Mobility and Aerodynamic  
231 Diameter Measurements. Part 1: Theory, *Aerosol Sci. Technol.*, 38, 1185–1205,  
232 doi:10.1080/027868290903907, 2004.
- 233 4 Draxler, R. R., and Rolph, G. D.: HYbrid Single-Particle Lagrangian Integrated Trajectory  
234 Model, In: National Air Quality Conference, NOAA Air Resource Laboratory,  
235 [https://www.arl.noaa.gov/documents/workshop/NAQC2007/HTML\\_Docs/index.html](https://www.arl.noaa.gov/documents/workshop/NAQC2007/HTML_Docs/index.html),  
236 2007.
- 237 5 Gong, X., Wang, Y., Xie, H., Zhang, J., Lu, Z., Wood, R., Stratmann, F., Wex, H., Liu, X.,  
238 and Wang, J.: Maximum supersaturation in the marine boundary layer clouds over the  
239 North Atlantic, *AGU Advances*, 4, e2022AV000855, doi.:10.1029/2022AV000855, 2023.

- 240 6 Heintzenberg, J., Covert, D., and Van Dingenen, R.: Size distribution and chemical  
241 composition of marine aerosols: a compilation and review, *Tellus B: Chem. Phys.*  
242 *Meteorol.*, 52, 1104–1122, doi:10.3402/tellusb.v52i4.17090, 2000.
- 243 7 Laing, J. R., Jaffe, D. A., and Sedlacek III, A. J.: Comparison of Filter-based Absorption  
244 Measurements of Biomass Burning Aerosol and Background Aerosol at the Mt. Bachelor  
245 Observatory. *Aerosol Air Qual. Res.*, 20, 663-678, doi:10.4209/aaqr.2019.06.0928, 2020.
- 246 8 Petters, M. D., and Kreidenweis, S. M.: A single parameter representation of hygroscopic  
247 growth and cloud condensation nucleus activity, *Atmos. Chem. Phys.*, 7, 1961-1971,  
248 doi:10.5194/acp-7-1961-2007, 2007.
- 249 9 Stein, A. F., Draxler, R. R., Rolph, G. D., Stunder, B. J., Cohen, M. D., and Ngan, F.:  
250 NOAA's HYSPLIT Atmospheric Transport and Dispersion Modeling System, *B. Am.*  
251 *Meteorol. Soc.*, 96, 2059-2077, doi:10.1175/bams-d-14-00110.1, 2015.
- 252 10 Wexler, A. S. and Clegg, S. L.: Atmospheric aerosol models for systems including the ions  
253  $H^+$ ,  $NH_4^+$ ,  $Na^+$ ,  $SO_4^{2-}$ ,  $NO_3^-$ ,  $Cl^-$ ,  $Br^-$ , and  $H_2O$ , *J. Geophys. Res.*, 107(D14), 4207,  
254 doi:10.1029/2001JD000451, 2002.